A Leucine Zipper-Like Sequence from the Cytoplasmic Tail of the HIV-1 Envelope Glycoprotein Binds and Perturbs Lipid Bilayers†

Yossef Kliger and Yechiel Shai*

Department of Membrane Research and Biophysics, Weizmann Institute of Science, Rehovot, 76100 Israel

Received December 2, 1996; Revised Manuscript Received February 19, 1997⊗

ABSTRACT: HIV-1 transmembrane envelope glycoprotein (gp41) has an unusually long cytoplasmic domain that has secondary associations with the inner leaflet of the membrane. Two highly amphiphatic α-helices in the cytoplasmic domain of gp41 have previously been shown to interact with lipid bilayers. We have detected a highly conserved leucine zipper-like sequence between the two α-helices. A peptide corresponding to this segment (residues 789−815, LLP-3) aggregates in aqueous solution, but spontaneously inserts into phospholipid membranes and dissociates into α-helical monomers. The peptide perturbs the bilayer structure resulting in the formation of micelles and other non-bilayer structures. Tryptophan fluorescence quenching experiments using brominated phospholipids revealed that the peptide penetrates deeply into the hydrophobic milieu of the membrane bilayer. The peptide interacts equally with zwitterionic and negatively-charged phospholipid membranes and is protected from proteolytic digestion in its membrane-bound state. Polarized attenuated total reflection Fourier transform infrared (ATR-FTIR) spectroscopy showed that the LLP-3 α-helix axis is about 70° from the normal to the membrane plane. The ATR-FTIR CH_2-stretching dichroic ratio increases when the peptide is incorporated into pure phospholipid membranes, further indicating that the peptide can deeply penetrate and perturb the bilayer structure. Integrating these data with what is already known about the membrane-associating features of adjacent segments, we propose a revised structural model in which a large portion of the cytoplasmic tail of the HIV-1 envelope glycoprotein is associated with the membrane.

HIV-1[1] envelope glycoprotein plays a critical role in the life cycle and biology of the virus. Initially synthesized as a single polypeptide precursor (gp160), the HIV-1 envelope glycoprotein forms oligomeric complexes in the golgi apparatus before cleavage into two non-covalently associated subunits, gp120 and gp41, by a host cell protease (Robey et al., 1985). gp120 is the outer surface glycoprotein and contains the sites necessary for viral binding to specific target cells (Lasky et al., 1987). gp41 has one transmembrane domain and is responsible for anchoring the envelope glycoprotein complex to the viral membrane, envelope glycoprotein oligomerization, and for the fusion process between viral and cell membranes or between infected and healthy cells (Veronese et al., 1985; Kowalski et al., 1987). The fusion process leads to syncitium formation of immune system cells, which is one of the causes for AIDS [reviewed in Levy (1993)]. Previous studies have focused on the hydrophobic amino terminal segment of gp41, namely, the "fusion peptide". Recent reports have indicated that other domains within viral fusion proteins are also important in the mediation of membrane fusion. For example, it appears that cytoplasmic and transmembrane domains are necessary components in the fusion process in both HIV-1 and influenza virus (Salzwedel et al., 1993; Kemble et al., 1994).

A striking feature of the HIV-1 envelope protein sequence is the unusual length (150 residues) of the region that follows its transmembrane domain (Wain-Hobson et al., 1985). This long cytoplasmic tail contains regions that associate with cellular membranes (Haffar et al., 1991), suggesting membrane-related functions which still are not clear. The cytoplasmic tail of gp41 does not affect proteolytic processing of the envelope glycoprotein, although it has some effect on the levels of surface protein expression and syncitium formation (Gabuzda et al., 1992; Owens & Rose, 1993). Moreover, amino acid replacements or deletions in this region affect T-cell killing (Fisher et al., 1986) and HIV infectivity and replication (Kowalski et al., 1987; Lee et al., 1989). Sodroski and colleagues have suggested that the carboxyl terminus of the cytoplasmic domain plays a role in HIV-1 entry such as in the uncoating or penetration of the viral core (Gabuzda et al., 1992) as opposed to receptor binding or membrane fusion. Furthermore, the cytoplasmic tail mediates polarized budding of HIV-1 in polarized epithelial cells (Lodge et al., 1994). The large hydrophobic moments of two amino acid segments from the carboxyl terminus of gp41 suggest membrane-related functions (Eisenberg & Wesson, 1990). Synthetic peptides corresonding to these regions could bind and perturb lipid bilayers (Fujii et al., 1992; Srinivas et al., 1992; Gawrisch et al., 1993) and were

† This work was supported in part by the Basic Research Foundation administered by the Israel Academy of Sciences and Humanities.

* To whom correspondence should be addressed. Tel: 972-8-9342711. FAX: 972-8-9344112. E-mail: bmshai@weizmann.weizmann.ac.il.

⊗ Abstract published in *Advance ACS Abstracts,* April 1, 1997.

[1] Abbreviations: ATR, attenuated total reflection; BOC, butyloxycarbonyl; CD, circular dichroism; diS-C_2-5, 3,3′-diethylthiodicarbocyanine iodode; FTIR, Fourier transform infrared; HEPES, *N*-(2-hydroxyethyl)piperazine-*N*′-2-ethanesulfonic acid; HIV, human immunodeficiency virus; HF, hydrogen fluoride; MLV, multilamellar vesicles; NBD-F, 4-fluoro-7-nitrobenz-2-oxa-1,3-diazole-4-yl; PAM, (phenylacetamido)methyl; PBS, phosphate-buffered saline, without Ca^{2+} and Mg^{2+}; PC, egg phosphatidylcholine; PS, phosphatidylserine; SUV, small unilamellar vesicles; TFA, trifluoroacetic acid; TFE, 2,2,2-trifluoroethanol.

S0006-2960(96)02935-2 CCC: $14.00

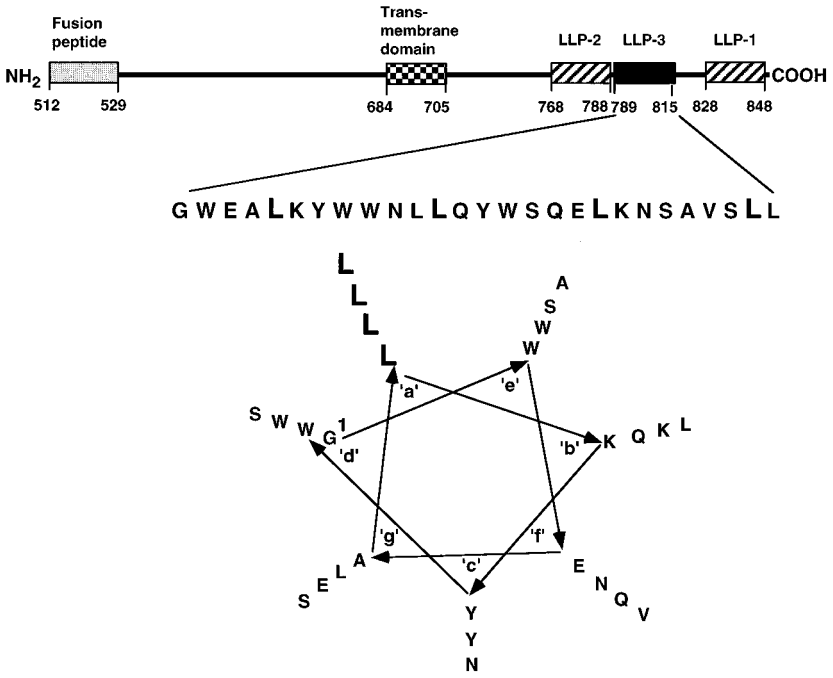

FIGURE 1: Top: Schematic representation of the transmembrane HIV-1 envelope glycoprotein (gp41) and the designation and the sequence of the peptide used. Bottom: Wheel projection of LLP-3. The amino acid sequence is displayed end-to-end down the axis of a schematic helix. The angle between every two consecutive amino acids is 102.9°. The helical wheel consists of seven corners, corresponding to the fit of seven amino acid residues into every two helical turns.

designated Lentivirus Lytic Peptide-1 (LLP-1) and LLP-2 (Miller et al., 1991, 1993a). Circular dichroism studies of LLP-1 and LLP-2 showed that their α-helicity increased with the addition of lipids, indicating the formation of lipid-associating amphiphatic helices (Srinivas et al., 1992; Gawrisch et al., 1993). Both LLP-1 and LLP-2 bind to calmodulin (Srinivas et al., 1993; Miller et al., 1993b; Tencza et al., 1995), and LLP-1, which is closer to the carboxyl terminus of gp41, has also been shown to inhibit the protein phosphorylation activity of protein kinase C (Ward et al., 1995).

In this study we have detected and characterized a highly conserved leucine zipper-like sequence in the cytoplasmic tail of gp41, located between LLP-1 and LLP-2 (aa 789−815, LLP-3 in Figure 1). We found that the peptide binds and perturbs negatively-charged and zwitterionic lipid membranes and forms oligomers in aqueous solution which dissociate to monomers upon their binding to the membrane. The membrane-bound monomers are α-helices oriented obliquely to the membrane plane as determined by polarized ATR-FTIR. The results are discussed in the light of a proposed model for the membrane association of gp41 cytoplasmic tail.

MATERIALS AND METHODS

Materials. BOC-amino acid PAM resins were purchased from Applied Biosystems (Foster City, CA), and BOC-amino acids were obtained from Peninsula Laboratories. Other reagents for peptide synthesis were obtained from Sigma. Egg phosphatidylcholine (PC) and phosphatidylserine (PS) from bovine spinal cord (sodium salt, grade I) were purchased from Lipid Products (South Nutfield, U.K.). 1-Palmitoyl-2-steroyl-(6,7, 9,10, or 11,12)-dibromo-*sn*-glycero-3-phosphocholines were purchased from Avanti Polar Lipids (Alabaster, AL). Cholesterol (extra pure) purchased from Merck (Darmstadt, Germany) was recrystallized twice from ethanol. 3,3′-Diethylthiodicarbocyanine iodide (diS-C_2-5), NBD-F (4-fluoro-7-nitrobenz-2-oxa-1,3-diazole), and tetramethylrhodamine were obtained from Molecular Probes (Eugene, OR). All other reagents were of analytical grade. Phosphate-buffered saline (PBS) was composed of NaCl (8 g/L), KCl (0.2 g/L), KH_2PO_4 (0.2 g/L), and Na_2HPO_4 (1.09 g/L), pH 7.4.

Peptide Synthesis and Fluorescent Labeling. LLP-3 (see Figure 1) was synthesized by a solid phase method on PAM-amino acid resins (0.15 mequiv) (Merrifield et al., 1982), as previously described (Shai et al., 1990). Another peptide designated the V2E mutant of the HIV-1 fusion peptide (sequence: AEGIGALFLGFLGAAGSTMGARSMTLTVQA-RQL) (Kliger et al., 1996) was also synthesized as a control. Labeling of the N-terminus of the peptides was achieved as previously described (Rapaport & Shai, 1991, 1992). Briefly, resin-bound peptides, with their amino acid side chains fully protected, were treated with trifluoroacetic acid (TFA) to remove the BOC protecting group from their N-terminal amino groups, while keeping all the other reactive amine groups of the attached peptides still protected. The resin-bound peptides were then reacted with the desired fluorescent probe and finally cleaved from the resins by HF, extracted with TFA, and precipitated with ether. This procedure yielded peptides selectively labeled with fluorescent probes at their N-terminal amino acid. The synthetic peptides were purified by reverse-phase HPLC on an analytical C_4 Vydac column 4.6 mm × 250 mm (pore size of 300 Å). The column was eluted in 40 min, at a flow rate of 0.6 mL/min, using a linear gradient of 25−80% acetonitrile in water in the presence of 0.05% TFA (v/v). The peptides were subjected to amino acid analysis to confirm their composition.

Preparation of Lipid Vesicles. Small unilamellar vesicles (SUV) were prepared from PC/PS/cholesterol (4:4:1 w/w) or from PC/cholesterol (8:1 w/w) by sonication as described

in detail (Shai et al., 1990). The cholesterol was included in order to reduce the curvature of the small unilamellar vesicles (Lelkes & Friedmann, 1984).

Rhodamine Fluorescence Dequenching Measurements. Rhodamine-labeled peptide (0.1 μM final concentration) was added to 2 mL of PBS, and rhodamine fluorescence emission was tracked. Proteinase K was added (5 μg), and a greater intensity of the fluorescence emission was observed as a result of the dequenching of the rhodamine fluorescence. More proteinase K was added until there was no further increase in the fluorescence emission. In other experiments, SUV (90 μM) were added to a rhodamine-labeled peptide and the emission maximum was tracked. More SUV were added until there was no further increase in the emission maxima. Excitation was set at 530 nm (10 nm slit), and emission was set at 582 nm (8 nm slit). All fluorescence measurements were performed at room temperature on a Perkin-Elmer LS-50B spectrofluorometer, using a magnetic stirrer.

Tryptophan Fluorescence Measurements. Tryptophan fluorescence increases with the increase in the environment hydrophobicity, and a blue shift of the emission maxima is observed. LLP-3 contains four tryptophan residues. Changes in the fluorescence of the peptide were measured following binding to lipid vesicles. LLP-3 (0.1 μM) was added to 2 mL of PBS, containing SUV (450 μM). Emission spectra were recorded, with excitation set at 280 nm, and compared to the emission spectra of the peptide in a liposome-free buffer.

NBD Fluorescence Measurements. NBD fluorescence increases with the increase in the environment hydrophobicity, and a blue shift of the emission maxima is observed. Changes in the fluorescence of the NBD-labeled peptide were measured following binding to lipid vesicles. NBD-labeled peptide (0.1 μM) was added to 2 mL of PBS, containing SUV (450 μM). Emission spectra were recorded, with excitation set at 467 nm, and compared to the emission spectra of the NBD-labeled peptide in a liposome-free buffer.

Membrane Partition of LLP-3. The degree of peptide association with lipid membranes was measured by titration of the NBD-labeled peptide (0.1 μM) with lipid vesicles in PBS. The fluorescence intensity was measured with excitation set at 467 nm (10 nm slit) and emission set at 530 nm (5 nm slit). The fluorescence values were corrected by taking into account the dilution factor corresponding to the addition of microliter amounts of liposomes and by subtracting the corresponding blank (buffer with the same concentration of vesicles). The binding isotherms were analyzed as partition equilibriums (Schwarz et al., 1986; Rizzo et al., 1987), as described in detail previously (Rapaport & Shai, 1991). Control experiments with unlabeled peptide using tryptophan as intrinsic fluoroprobes, yielded very similar results suggesting that the NBD moiety does not interfere with the peptide−lipid interaction.

Resonance Energy Transfer Measurements. Fluorescence resonance energy transfer was measured using NBD-labeled peptide serving as a donor and rhodamine-labeled peptide as an energy acceptor (Fung & Stryer, 1978; Gazit & Shai, 1993). Fluorescence spectra were obtained at room temperature, with excitation set at the NBD maximum absorption wavelength (467 nm). In a typical experiment, a donor peptide (final concentration 0.07 μM) was added to a dispersion of PC/PS/cholesterol (4:4:1 w/w) SUV (180 μM) in PBS, followed by the addition of the acceptor peptide in several sequential doses. Fluorescence spectra were obtained before and after addition of the acceptor. The efficiency of energy transfer (E) was determined by measuring the decrease in the quantum yield of the donor as a result of the presence of the acceptor. E was determined experimentally from the ratio of the fluorescence intensities of the donor in the presence (I_{da}) and in the absence (I_d) of the acceptor, at the donor's maximum emission wavelength (530 nm). The percentage of transfer efficiency (E, in %), is given by

$$E = (1 - I_{da}/I_d) \times 100$$

Correction for the contribution of acceptor emission as a result of direct excitation was made by subtracting the signal produced by the acceptor-labeled analogue alone. The contributions of the buffer and vesicles were also subtracted from all measurements.

Circular Dichroism (CD) Spectroscopy. CD spectra were obtained using a Jasco J-500A spectropolarimeter. Spectra were scanned in a capped quartz optical cell with a 2 mm path length, at room temperature. Each spectrum was the average of eight scans at wavelengths of 250−190 nm. Fractional helicities, f_h (Wu et al., 1981), were calculated as follows:

$$f_h = \frac{[\theta]_{222} - [\theta]^0_{222}}{[\theta]^{100}_{222} - [\theta]^0_{222}}$$

where $[\theta]_{222}$ is the experimentally observed absolute mean residue ellipticity at 222 nm, and values for $[\theta]^0_{222}$ and $[\theta]^{100}_{222}$, corresponding to 0% and 100% helix content at 222 nm, are estimated at 2000 and 32 000 deg·cm^2/dmol, respectively.

Accessibility of Membrane-Bound Peptide to Proteolytic Digestion. The accessibility of NBD-labeled LLP-3 to proteolytic digestion when bound to lipid vesicles was investigated. Lipid vesicles (90 μM) were added to NBD-labeled LLP-3 (0.1 μM, in PBS). After 15 min, proteinase K (1 μg/400 μL final concentration) was added. Fluorescence emission as a function of time was obtained before and after the addition of the enzyme. In control experiments, to check the efficiency of the enzyme, LLP-3 was initially incubated with proteinase K in aqueous solution, followed by the addition of the liposomes. In another control experiment SUV were added to NBD-labeled HIV-V2E fusion peptide in PBS, followed by the addition of proteinase K. Excitation, 467 nm, slit, 10 nm; emission, 530 nm, slit, 8 nm.

Tryptophan Quenching using Brominated Phospholipids. Brominated-PC employed as quenchers of tryptophan fluorescence are suitable for probing the peptide insertion into membrane because they act over a very short distance (apparent $R_0 = 9$ Å), decrease with r^6 dependence, and do not significantly perturb the membrane (Bolen & Holloway, 1990; De Kroon et al., 1990; Killian et al., 1990; Gonzalez et al., 1992). LLP-3, which contains four tryptophan residues, was added (final concentration of 0.5 μM) to 400 μL suspensions of either PC/cholesterol (8:1 w/w) or PS/PC/cholesterol (4:4:1 w/w) SUV (450 μM) in PBS, establishing a lipid to peptide molar ratio of 900:1. The kinetics of the binding was very rapid (see Figure 4B). After 2 min,

an emission spectrum (6 nm slit) of the tryptophan was recorded with excitation set at 280 nm (8 nm slit). In three separate experiments, SUV containing 40% of 6,7-brominated-PC, 9,10-brominated-PC, or 11,12-brominated-PC were used. For comparison, SUV with no brominated-PC were used.

ATR-FTIR Measurements. Spectra were obtained with a Perkin-Elmer 1600 FTIR spectrometer coupled with an ATR device. For each spectrum, 512 or 1024 scans were collected, with resolution of 2 or 4 cm^{-1}. Samples were prepared as previously described (Gazit et al., 1996); briefly, a mixture of PC (1 mg) alone or with peptide (100 μg) was deposited on a germanium prism (52 × 20 × 2 mm). The aperture angle of 45° yielded 25 internal reflections. Lipid−peptide mixtures were prepared by dissolving them together in a 1:2 MeOH/CH_2Cl_2 mixture and drying under a stream of nitrogen. To determine the amide I and II absorption peaks of the peptide, polarized spectra were recorded and the respective pure phospholipid in each polarization were subtract to yield the difference spectra. The background for each spectrum was a clean germanium prism. Hydration of the sample was achieved by addition of 10 μL of ^2H_2O into a rubber chamber placed around the prism in the ATR casting. Spectra under a ^2H_2O atmosphere ("wet" conditions) were taken after 2 and 4 h. No significant differences between the spectra in the CH_2 stretching and amide I and II regions were observed, suggesting that maximal hydration occurred within 2 h. Furthermore, the amide I/amide II ratio remained constant suggesting that deuteration was complete. Any contribution of the ^2H_2O vapor to the absorbance spectra near the amide peak region was eliminated by the subtraction of the spectra of pure lipid saturated with ^2H_2O under the same conditions.

ATR-FTIR Data Analysis. The ATR electric fields of incident light were calculated as follows (Harrick, 1967; Ishiguro et al., 1993).

$$E_x = \frac{2\cos\theta\sqrt{\sin^2\theta - n_{21}^2}}{\sqrt{(1-n_{21}^2)[(1+n_{21}^2)\sin^2\theta - n_{21}^2]}}$$

$$E_y = \frac{2\cos\theta}{\sqrt{1-n_{21}^2}}$$

$$E_z = \frac{2\sin\theta\cos\theta}{\sqrt{(1-n_{21}^2)[(1+n_{21}^2)\sin^2\theta - n_{21}^2]}}$$

where θ is the angle of a light beam to the prism normal at the point of reflection (45°), and $n_{21} = n_2/n_1$ [n_1 and n_2 are the refractive indices of Ge (taken as 4.03) and the membrane sample (taken as 1.5), respectively]. Under these conditions, E_x, E_y, and E_z are 1.40, 1.52, and 1.64, respectively. The electric field components together with the dichroic ratio (defined as the ratio between absorption of parallel (to a membrane plane), A_p, and perpendicularly polarized incident light, A_s) are used to calculate the orientation order parameter, f, by the following formula:

$$R^{ATR} = \frac{A_p}{A_s} = \frac{E_x^2}{E_y^2} + \frac{\{(E_z^2/E_y^2)[f\cos^2\alpha + ((1-f)/3)]\}}{[(f\sin^2\alpha)/2 + (1-f)/3]}$$

where α is the angle between the transition moment of the amide I vibration of an α-helix and the helix axis. We used the value of 27° for α as was previously suggested (Rothschild & Clark, 1979; Ishiguro et al., 1993). The orientation order parameter, f, allows us to calculate the average angle of the peptide α-helices relative to the membrane normal, γ, by the following formula:

$$f = \frac{3\cos^2\gamma - 1}{2}$$

Lipid order parameters were obtained from the symmetric (~2853 cm^{-1}) and asymmetric (~2922 cm^{-1}) lipid stretching mode using the same equations, setting $\alpha = 90°$ (Ishiguro et al., 1993).

Membrane Permeability Studies. Membrane destabilization, reflected by the collapse of the diffusion potential, was detected fluorimetrically as previously described (Loew et al., 1983; Shai et al., 1990). In a typical experiment, 4 μL (28 μg) of a liposome suspension, prepared in "K^+ buffer" (50 mM K_2SO_4, 25 mM HEPES-sulfate, pH 6.8), were diluted in 1 mL of isotonic K^+ free buffer (50 mM Na_2SO_4, 25 mM HEPES-sulfate, pH 6.8), to which the potential-sensitive fluorescent dye, diS-C_2-5 (M_r = 492) was then added. Subsequent addition of valinomycin created a negative diffusion potential inside the vesicles by a selective efflux of K^+ ions, resulting in a quenching of the dye's fluorescence. 15 min after fluorescence was stabilized, peptides were added. Peptide-induced membrane permeability toward all the ions in the solution caused dissipation of the diffusion potential, monitored by an increase of fluorescence. Fluorescence was monitored using excitation set at 620 nm and emission at 670 nm. The percentage of fluorescence recovery (F_t, in %) was defined by

$$F_t = [(I_t - I_o)/(I_f - I_o)] \times 100$$

where I_t = fluorescence observed after adding the peptide, at time t, I_o = the initial fluorescence (after addition of valinomycin), and I_f = total fluorescence prior to the addition of valinomycin.

Negative Staining Electron Microscopy (EM). The effect of the peptides on lipid suspensions was examined by negative staining EM. Multilamellar vesicles (MLV) were prepared from dry phospholipids with or without LLP-3. The peptide to lipid molar ratio was 1:750. A drop containing MLV alone, or a mixture of MLV and peptide, was deposited on a carbon-coated grid and negatively stained with 2% uranyl acetate. The grids were examined using a JEOL JEM 100B electron microscope (Japan Electron Optics Laboratory Co., Tokyo, Japan).

RESULTS

Identification of a Highly Conserved Leucine Heptad Repeat Sequence in the Cytoplasmic Tail of HIV-1 Transmembrane Glycoprotein. The absence of 3′ → 5′ exonuclease activity of reverse transcriptase causes a mutation frequency 1000 times higher than that of DNA polymerase. Therefore, it is possible to predict amino acid sequences vital for the retroviruses' life cycle on the basis of conserved sequences. Sequence alignment [using the PileUp program of the Wisconsin Package, Version 8, September 1994, Genetics Computer Group (GCG) 575 Science Drive, Madison, WI, 53711] of the cytoplasmic portion of gp41

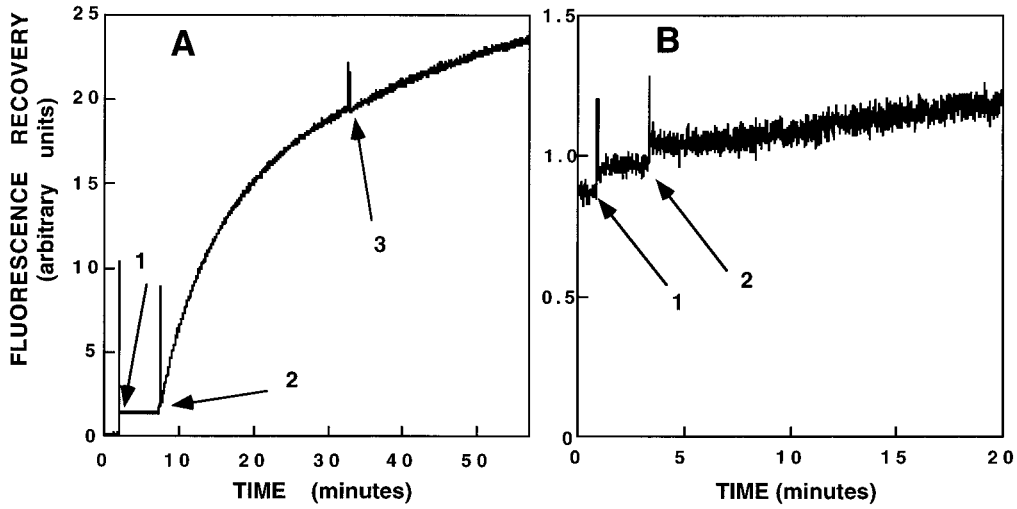

FIGURE 2: Association of LLP-3 in aqueous solution. (A) Proteolytic digestion of LLP-3 in aqueous solution by proteinase K. Rhodamine-labeled LLP-3 (0.1 μM) was added to 2 mL of PBS at the first point, followed by addition of 20 μL of proteinase K solution (0.25 μg/μL) at the second and the third points. Excitation, 530 nm; emission, 582 nm. (B) Addition of unlabeled LLP-3 to rhodamine-labeled LLP-3 (0.1 μM). The unlabeled peptide concentration was 0.03 μM at the first point and 0.1 μM at the second point. Excitation, 530 nm; emission, 582 nm.

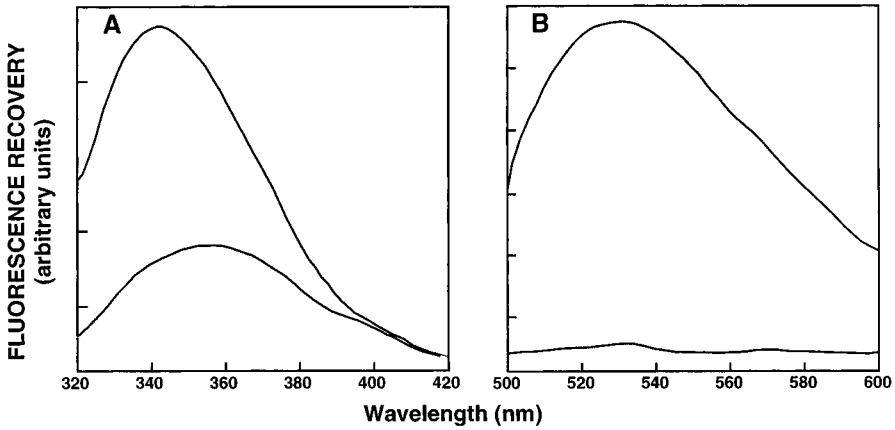

FIGURE 3: Fluorescence emission blue shift due to binding of LLP-3 to membrane. (A) Tryptophan fluorescence spectra of LLP-3 (0.1 μM) in buffer (bottom line) or in the presence of 450 μM liposomes (top line). The excitation wavelength was set at 280 nm, and emission was scanned from 320 to 420 nm. (B) Fluorescence emission spectra of NBD-labeled LLP-3 (0.1 μM) in buffer (bottom line) or in the presence of 450 μM lipsomes (top line). The excitation wavelength was set at 467 nm, and emission was scanned from 500 to 600 nm.

reveals that there is a highly conserved heptad repeat motif at amino acid residues 789−815 (designated LLP-3 in Figure 1). Heptad repeats are characterized by hydrophobic amino acids in the "a" and "d" positions of the helix. In LLP-3, all the "a" positions are leu, and two of the "d" positions are trp residues. Comparison of all gp41 sequences from SwissProt reveals that LLP-3 is highly conserved with respect to adjacent sequences. All leucine residues are conserved among all the HIV sequences, and this motif is even conserved in some strains of a related virus, SIV, although there are some L to I replacements. Kernel density analysis of the HIV-1 envelope glycoprotein supports the traditional alignment results (Lauder et al., 1996). None of the sequence variations altered the leucine heptad repeat, suggesting a strong selective pressure to conserve this motif despite other extensive sequence variations in HIV. The function of this motif is unknown. To elucidate its possible role in the life cycle of the virus, we have investigated the properties of LLP-3, a synthetic peptide identical to this segment.

Self-Association of LLP-3 in Aqueous Solution. LLP-3 self-association in solution was tested using a rhodamine-labeled peptide. Since the fluorescence of rhodamine is quenched when several molecules are in close proximity, an increase in fluorescence is expressed when rhodamine-labeled peptide aggregates dissociate, a process that occurs when the peptide is enzymatically cleaved. The fluorescence of rhodamine-labeled LLP-3 (0.1 μM as determined by absorbance at 567 nm in DMSO) added to PBS, was very low in comparison to other rhodamine-labeled peptides at the same concentration, suggesting that the formation of LLP-3 aggregates in aqueous solution. Furthermore, there was a large increase (>20-fold) in fluorescence emission (Figure 2A) following the addition of proteinase-K to LLP-3 (0.1 μM). Increases in the quantum yield were also observed when unlabeled peptide was added to the rhodamine-labeled analogue (Figure 2B). These data suggest that there is an equilibrium between aggregation states of LLP-3 in aqueous solution.

Interaction of LLP-3 with Phospholipid Membranes. Experiments were carried out with either neutral phospholipid PC/cholesterol (8:1 w/w) or negatively-charged PS/PC/cholesterol (4:4:1 w/w) vesicles. Identical results were obtained using both types of membranes.

Blue Shift of LLP-3 Fluorescence Emission Due to Membrane Binding. LLP-3 interaction with lipid vesicles was detected by the change in its tryptophans fluorescence,

which is environmentally sensitive. The increase in the quantum yield and a shift of the emission maximum wavelength of the intrinsic tryptophans (Figure 3A), indicates that the tryptophan moieties of the peptide entered a hydrophobic environment. Similar experiments were carried out using LLP-3 labeled at its N-terminus with NBD, a highly environmentally sensitive probe (Figure 3B). Previously, NBD has been used to probe the hydrophobicity of its microenvironment in investigations of the interactions of various peptides with membranes (Frey & Tamm, 1990; Rapaport & Shai, 1991). When LLP-3 bound to membranes, there was a large increase in the quantum yield and a blue shift of the maximum emission wavelength to 530 nm. Blue shifts of these magnitudes are observed when surface-active NBD-labeled peptides interact with lipid membranes (Rapaport & Shai, 1991; Gazit et al., 1994) and are consistent with the NBD probe being located near the membrane surface (Rajarathnam et al., 1989). In our experiments, the lipid/peptide molar ratio was extremely high (4500:1) so that spectral contributions of free peptides are negligible.

Membrane Partition of LLP-3. Analyses of the membrane-bound fraction of LLP-3 as a function of the lipid to peptide molar ratio revealed that the partitioning of the peptide in the membrane is similar with both PC/cholesterol (8:1 w/w) and PC/PS/cholesterol (4:4:1 w/w) vesicles. Similar results were observed when measuring the NBD fluorescence of NBD-labeled LLP-3. More than 75% of the peptide bound to the membrane (data not shown) when the lipid to peptide molar ratio was 500. We could not derive the membrane partition coefficient from our data (Schwarz et al., 1986; Rizzo et al., 1987) because LLP-3 aggregates in aqueous solution. If we rule out the changes in the emission caused by aggregation, we would obtain K_p values in the range of 10^4 M^{-1}.

LLP-3 Is a Monomer in Its Membrane-Bound State. When rhodamine-labeled monomers are aggregated and the rhodamine probes are close to each other, the result is self-quenching of the emission fluorescence. Following the addition of lipid vesicles, more than a 20-fold increase in the quantum yield of rhodamine-labeled LLP-3 was observed (Figure 4A), which indicates dissociation of LLP-3 aggregates. To ascertain whether the increased fluorescence, or dequenching, results from the dissociation of LLP-3 oligomers and not from changes in the probe's environment (though, rhodamine is barely sensitive to its environment hydrophobicity), we have compared the rhodamine-labeled LLP-3 dissociation rate with the kinetics of membrane binding. An immediate large increase in the quantum yield of the tryptophan fluorescence was observed upon the addition of lipid vesicles to LLP-3 (Figure 4B). Similar kinetics was observed using NBD-labeled LLP-3 (data not shown). Tryptophan and NBD fluorescence are much more sensitive than rhodamine to the hydrophobicity of their environment. If we compare this rapid binding (Figure 4B) to the kinetics of the fluorescence dequenching of rhodamine-labeled LLP-3, followed by the addition of equal amounts of lipid vesicles (Figure 4A), it is possible to conclude that when LLP-3 is exposed to membranes, immediate binding takes place and is followed by a much slower process of oligomeric dissociation.

Resonance energy transfer experiments were further carried out to find whether LLP-3 dissociates into monomers or alternatively to smaller aggregates. NBD-labeled LLP-3 served as a donor, and rhodamine-labeled LLP-3 served as an energy acceptor. The results show that the efficiency of the energy transfer is close to the theoretically calculated values assuming a random distribution of donors and acceptors (Gazit & Shai, 1993) (Figure 4C, dashed line).

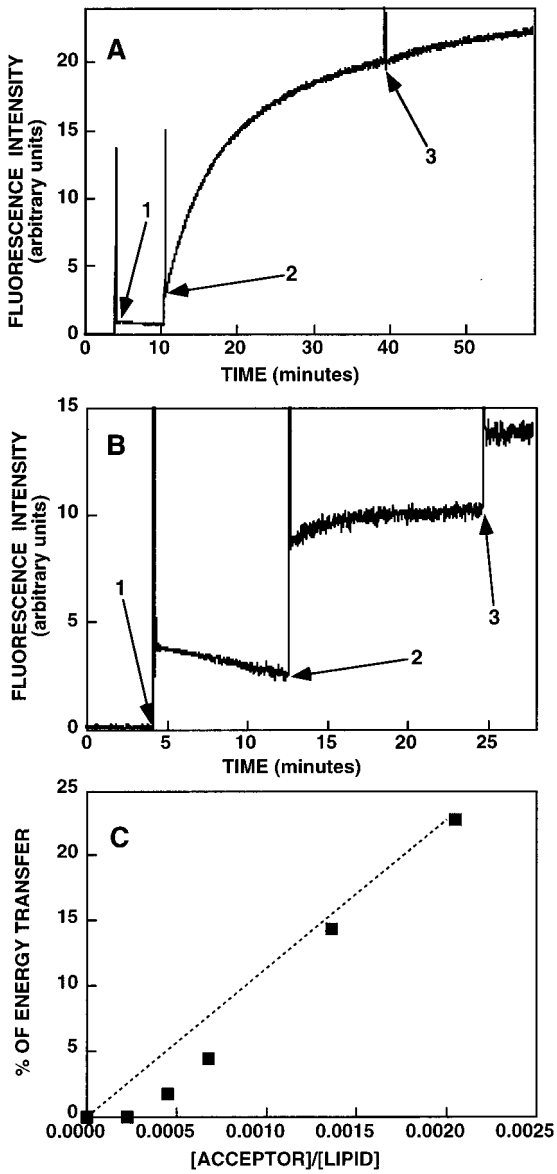

FIGURE 4: Dissociation of the LLP-3 oligomer after membrane binding. (A) Rhodamine-labeled LLP-3 (0.1 μM) was added to 2 mL of PBS at the first point, followed by the addition of lipid vesicles (90 μM each time) at the second and third points. Excitation, 530 nm; emission, 582 nm. (B) Instantaneous binding of LLP-3 to lipid vesicles. LLP-3 (0.1 μM) was added to 2 mL of PBS at the first point, followed by the addition of lipid vesicles (90 μM) at the second and third points. Changes in the tryptophan fluorescence were measured. Excitation, 280 nm; emission, 340 nm. (C) Theoretically and experimentally derived percentage of energy transfer. Transfer efficiencies between donor (NBD-labeled peptide) and acceptor (rhodamine-labeled peptide) LLP-3 are plotted versus the bound-acceptor/lipid molar ratio (filled squares). A theoretical plot showing energy transfer efficiency as a function of the surface density of the acceptors, assuming random distribution of donors and acceptors monomers (Fung & Stryer, 1978) and R_o = 51 Å (Gazit & Shai, 1993), is given for comparison (dashed line). The excitation wavelength was set at 467 nm; emission was scanned from 500 to 600 nm, and the energy transfer efficiency was calculated using the decrease in the donor's emission maxima (530 nm) as a result of addition of acceptor as described in detail in Methods.

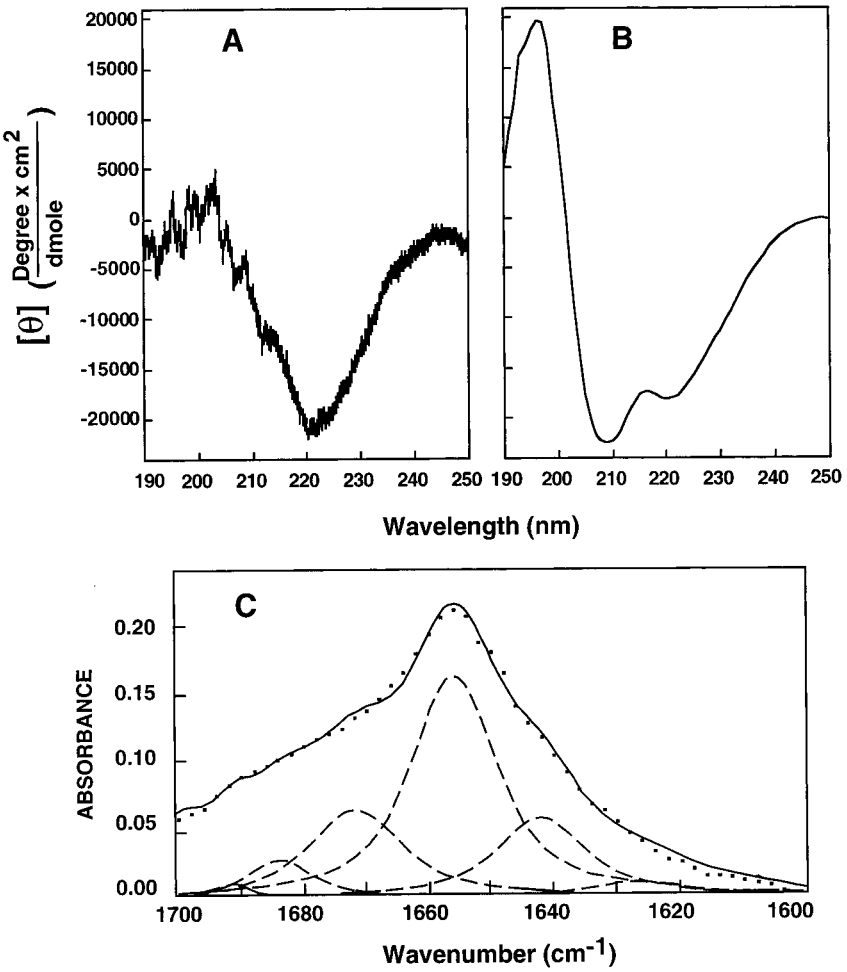

FIGURE 5: Secondary structure of LLP-3 as determined by CD and FTIR spectroscopy. (A) CD spectrum of LLP-3 incorporated into small unilamellar vesicles. Peptide concentration was 21 μM, and the peptide to lipid molar ratio was 1:47. (B) CD spectrum of LLP-3 (13 μM) in 40% TFE. (C) FTIR spectra deconvolution of the amide I band of LLP-3 (1700−1600 cm^{-1}). The component peaks are the result of curve-fitting using a Voigt line shape. The amide I frequencies characteristic of the various secondary structure elements were taken from Jackson and Mantsch (1995). The sum of the fitted components superimposes on the experimental amide I region spectrum. (···) Experimental FTIR spectrum; (- - -) the fitted components; (—) the sum of the fitted components. 100 μg of LLP-3 and 1 mg of PC were used for each scan (peptide to lipid molar ratio was 1:42).

These data indicate that LLP-3 is a monomer in its membrane-bound state.

Secondary Structure of LLP-3. LLP-3 cannot be solubilized in aqueous solution at concentrations necessary for CD measurements. We therefore, could only investigate the secondary structure of the peptide in its membrane-bound state. When LLP-3 is incorporated into PC/PS (1:1 w/w) vesicles, it adopts a partial α-helical conformation (Figure 5A). The spectra fits indicated α-helical content of approximately 63%. At wavelengths lower than 215 nm, the curve was noisy due to the vesicles' light scattering. Therefore, we repeated measurements with LLP-3 dissolved in 40% trifluoroethanol (TFE), a membrane-mimetic environment. Double minima at 222 and 208 nm are quite apparent, and the spectral fits indicate α-helical content of about 53% (Figure 5B). To confirm the α-helical conformation revealed by CD, FTIR spectroscopy was used. The amide I region between 1648 and 1660 cm^{-1} is characteristic of α-helical structure (Jackson & Mantsch, 1995). A spectrum of the amide I region for LLP-3 bound to a dry PC multibilayer is shown in Figure 5C. Deconvolution of the amide I region was performed using PEAKFIT, and the α-helix content was 54% ± 3%. Experiments were repeated using dry film samples to which D_2O was added to simulate more biologically relevant conditions. No significant changes between the dry and wet conditions were obtained.

Protection of Membrane-Bound LLP-3 from Enzymatic Digestion. To test whether membrane-bound LLP-3 is protected from enzymatic digestion, a nonspecific protease, proteinase K, was added to a mixture of NBD-labeled LLP-3 and lipid vesicles. The results indicate that membrane-bound LLP-3 is highly protected against enzymatic digestion (Figure 6A). When LLP-3 was initially incubated with proteinase K, prior to the addition of lipid vesicles, we found that the peptide was digested by the protease (Figure 6B). A control peptide, the V2E mutant of the fusion peptide of gp41, which also binds strongly to lipid vesicles, was susceptible to the enzyme in its membrane-bound state (Figure 6C). Enzymatic cleavage of V2E peptide results in small peptidic fragments with greatly reduced membrane affinity. These fragments dissociate from the membrane causing a decrease in the fluorescence intensity of NBD.

Tryptophan Quenching using Brominated Phospholipids. The intrinsic tryptophan fluorescence of LLP-3 was used to evaluate the degree of penetration of the peptide to the membrane bilayer. A naturally occurring tryptophan in a protein or peptide can serve as an intrinsic probe for its localization within the membrane. LLP-3 contains four

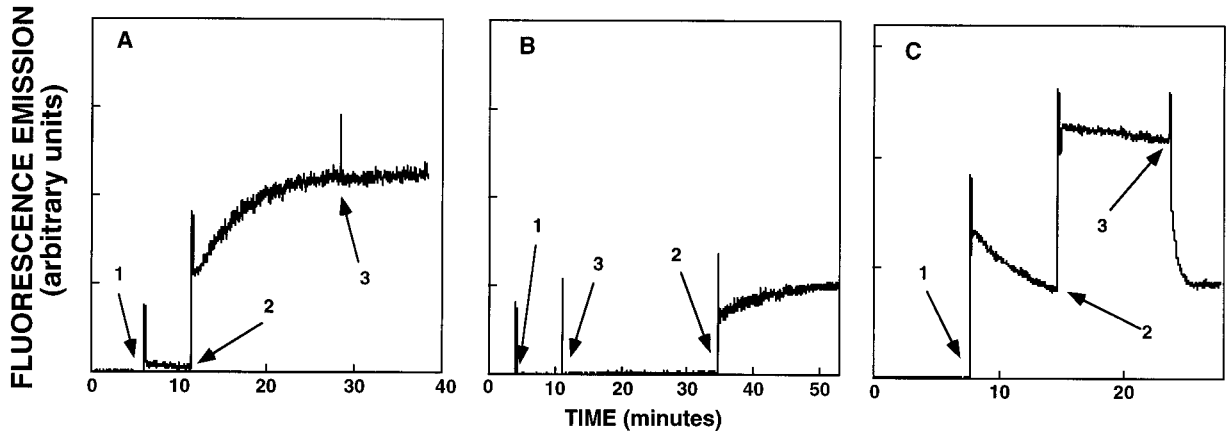

FIGURE 6: (A) Protection of membrane-bound NBD-labeled LLP-3 against proteolytic digestion. The fluorescence emission of the environmentally sensitive NBD of NBD-labeled peptide was monitored at 530 nm with the excitation set at 467 nm: (1) addition of 0.1 μM NBD-labeled LLP-3; (2) addition of 90 μM lipid vesicles; (3) addition of the nonspecific protease, proteinase K (1 μg/400 μL). (B) A control experiment to check the efficiency of proteinase K in digesting LLP-3 in aqueous solution. The numbers are as described in panel A. This time the enzyme was added to LLP-3 22 min before the addition of the vesicles. (C) For a comparison, NBD-labeled V2E fusion peptide served as a control peptide: (1) addition of 0.1 μM NBD-labeled V2E fusion peptide; 2 and 3 are as described in panels A and B.

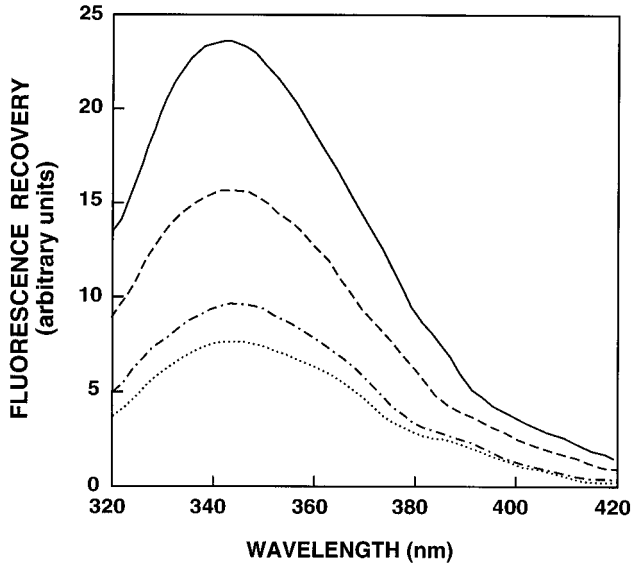

FIGURE 7: Tryptophan quenching using brominated phospholipids. Tryptophan fluorescence spectra of LLP-3 (0.5 μM) in the presence of PC/cholesterol (8:1 w/w) liposomes (—) or in the presence of PC/cholesterol (8:1 w/w) containing 40% 11,12-brominated-PC (- - -), 40% 9,10-brominated-PC (-·-), or 40% 6,7-brominated-PC (···). The excitation wavelength was set at 280 nm, and emission was scanned from 320 to 420 nm.

tryptophans, three in the middle of the peptide and the fourth near the amino terminus. Br quenches tryptophan fluorescence with an r^6 dependence and an apparent R_0 of 9 Å (Bolen & Holloway, 1990). Bromolipids [1-palmitoyl-2-(dibromostearoyl)phosphatidylcholine] with bromines at the 6,7-, 9,10-, and 11,12-positions were used as molecular rulers to examine the fluorescence quenching of LLP-3. The greatest quenching of tryptophan fluorescence was observed using 6,7-brominated-PC, a lesser degree of quenching with 9,10-brominated-PC, and the least amount of quenching with 11,12-brominated-PC (Figure 7). The peptide to lipid molar ratio in these experiments was kept very low (1:900), so no membrane perturbation is expected (Figure 9). Using a surface-localized peptide (M0), quenching was observed with 6,7-Br-PC and 9,10-Br-PC but was not observed with 11,12-Br-PC (Ben-Efraim & Shai, 1996). In the case of LLP-3, even PC with Br at its 11 and 12 acyl chain carbons causes quenching of its fluorescence, indicating that at least one of its tryptophan residues is located deeply within the hydrophobic core of the membrane. Similar results were revealed using PS/PC/cholesterol (4:4:1 w/w) liposomes containing 40% of these brominated PC. These data are consistent with results obtained with enzymatic digestion experiment (Figure 6A), which suggest that while the amino terminus of LLP-3 is close to the surface of the membrane (as revealed from the NBD fluorescence, Figure 3B), other parts of the peptide are inserted within the hydrophobic milieu of the membrane bilayer.

Orientation of the Phospholipid Membrane and the Effect of LLP-3 Binding on the Acyl Chain Order. Polarized ATR-FTIR was used to determine the orientation of the lipid membrane. The symmetric [$\nu_{sym}(CH_2) \sim 2850$ cm^{-1}] and the antisymmetric [$\nu_{antisym}(CH_2) \sim 2920$ cm^{-1}] vibrations of lipid methylene C−H bonds are perpendicular to the molecular axis of a fully extended hydrocarbon chain. Thus, measurements of the dichroism of infrared light absorbance can reveal the order and orientation of the membrane sample relative to the prism surface. Figure 8A shows that ATR dichroism spectra of parallel and perpendicular polarized ATR-FTIR absorbance spectra between 2800 and 3000 cm^{-1}. R values based on the stronger $\nu_{antisym}(CH_2)$ were 1.40 ± 0.06. Using $\nu_{sym}(CH_2)$ instead, somewhat lower R values, $R = 1.29 \pm 0.05$, were obtained. The data indicate that the phospholipid membrane is well ordered, permitting the orientation of the peptide to be determined. Similar results have been obtained by others (Fringeli & Günthard, 1981; Yang et al., 1987; Ishiguro et al., 1993; Gazit et al., 1996). On the basis of the dichroic ratio of lipid stretching, the corresponding orientation order parameter, f, was calculated to be 0.46 ± 0.05 and a tilt angle in the range of 36.9 ± 2.1° was calculated for the main transition moments of the axis of the lipids. The observed antisymmetric and symmetric peaks at 2921.9 ± 0.2 and 2852.7 ± 0.3 cm^{-1}, respectively (Figure 8A), indicate that the membranes were predominantly in a liquid-crystalline phase (Cameron et al., 1980; Ishiguro et al., 1993), just like biological cell membranes. Thus, the lipid multibilayer used in our study was well oriented and in a liquid-crystalline phase.

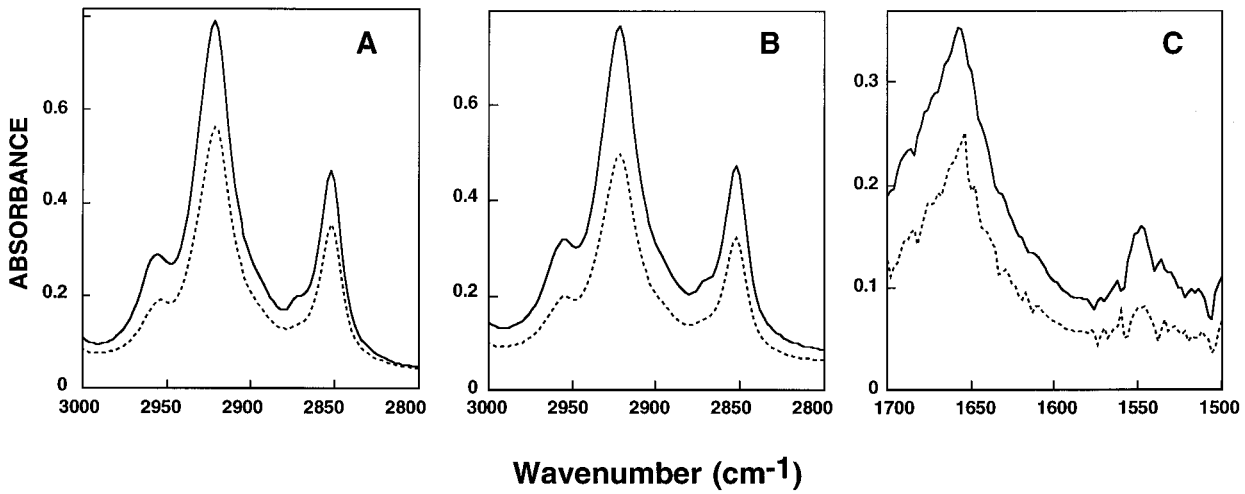

FIGURE 8: (A) ATR dichroism of parallel and perpendicular polarized ATR-FTIR absorbance spectra between 3000 and 2800 cm^{-1} for the lipid CH_2 symmetric and antisymmetric vibration of PC multibilayers. The top line is for the P component of polarized incident light (an electric vector oscillates perpendicular to the Ge prism or membrane plane), and the bottom line is for the S (parallel) component. (B) ATR dichroism spectra of parallel and perpendicular polarized ATR-FTIR absorbance spectra between 3000 and 2800 cm^{-1} for the lipid CH_2 symmetric and antisymmetric vibration of PC multibilayers incorporated with LLP-3. The top line is for the P component of polarized incident light (an electric vector oscillates perpendicular to the Ge prism or membrane plane), and the bottom line is for the S (parallel) component. (C) ATR dichroism spectra of parallel and perpendicular polarized ATR-FTIR absorbance spectra between 1700 and 1500 cm^{-1} for the amide I and II absorbance regions of LLP-3 incorporated into PC multibilayers. The top line is for the P component of polarized incident light (an electric vector oscillates perpendicular to the Ge prism or membrane plane), and the bottom line is for the S (parallel) component. 100 μg of LLP-3 and 1 mg of PC were used for each scan (peptide to lipid molar ratio was 1:42).

The effect of LLP-3 on the multibilayer acyl chains order can be estimated by comparing the CH_2-stretching dichroic ratio of pure phospholipid multibilayers (Figure 8A) with that obtained with membrane-bound LLP-3 (Figure 8B). The results indicate that LLP-3 incorporation into the membrane increases R values to 1.54 $\pm$ 0.02, based on the stronger $\nu_{antisym}(CH_2)$, and 1.46 $\pm$ 0.01 based on $\nu_{sym}(CH_2)$. These data suggest that LLP-3 penetrates deeply into the hydrocarbon core of the membrane and are consistent with protection of membrane-bound LLP-3 from enzymatic digestion (Figure 6) and the results obtained from tryptophan quenching experiments (Figure 7).

Orientation of LLP-3 in Its Membrane-Bound State. Polarized ATR-FTIR was used to determine the orientation of membrane-bound LLP-3. Films of the peptide incorporated into phospholipids were disposed on a germanium prism. Figure 8C shows the ATR-FTIR absorbance spectra of LLP-3 in the amide I and II regions, perpendicular to the membrane surface, A_p (top curve), and parallel to it, A_s (bottom curve). The amide I region was deconvoluted using the program PEAKFIT, using either Lorenzian or Voigt line shapes. The α-helix was the dominant component, 50−60% of total area. Therefore, R^{ATR} was calculated using the height of the α-helical component of the amide I region and was equal to 1.36 $\pm$ 0.05. The corresponding order parameter, f, was equal to -0.33 ± 0.03, and the angle of the peptide relative to the membrane normal was calculated as 70.4 $\pm$ 1.9. The calculated orientation angle of LLP-3 should not be treated as a fixed value but rather as an indicator influenced by several factors, including the angle between the helix axis and the dipole moment of the amide I. Values ranging from 24 to 40° are being reported in the literature (Miyazawa & Blout, 1961; Bradbury et al., 1962). For $\alpha = 24°$, f is -0.29 and $\gamma = 68°$ to the membrane normal. When α is taken to be 40°, f is calculated to be -0.6, and that is more than the -0.5 allowed for a totally parallel helical orientation. We have used $\alpha = 27°$ as suggested by Rothschild & Clark (1979) and Ishiguro et al. (1993), hence $f = -0.33$ and $\gamma = 70°$. In addition, it is worth noting that the results describe only the α-helix components of LLP-3, which are about 50−60% of the peptide structure. Anyway, the results obtained clearly indicate that LLP-3 does not expand the membrane but is in a parallel or an oblique orientation to the membrane plane.

Membrane Permeability Studies. To study the potential of LLP-3 to destabilize lipid bilayers, we tested its ability to dissipate the diffusion potential in SUV prepared from PC/PS/cholesterol (4:4:1 w/w) vesicles. Increasing concentrations of peptides were mixed with vesicles, pretreated with the fluorescent dye, diS-C_2-5, and valinomycin. The kinetics of fluorescence recovery was monitored (Figure 9A), and fluorescence levels obtained after 10 min are represented as a function of the lipid/peptide molar ratio in Figure 9B. The slow kinetics of membrane permeation suggests that LLP-3 does not form pores in the membrane (Parente et al., 1990; Rapaport et al., 1996). This is consistent with the energy transfer results which have revealed that LLP-3 is a monomer in its membrane-bound state (Figure 4C). An inactive mutant of gp41 fusion peptide (Kliger et al., 1996), and the highly active neurotoxin, pardaxin (Oren & Shai, 1996) served as control peptides. Similar results were obtained using PC/cholesterol (8:1 w/w) SUV (data not shown). Thus, LLP-3 can strongly destabilize both neutral and negatively-charged membranes. Similar results are also obtained with rhodamine-labeled and NBD-labeled LLP-3 (data not shown) indicating that fluorescently labeled analogues can be used to replace LLP-3.

Electron Microscopy. To confirm that the dissipation of the membrane potential is a result of membrane destruction and not only a result of pore formation, PC/cholesterol (10:1) MLV with or without LLP-3 were visualized with negative staining electron microscopy. Figure 10 shows representative micrographs of the MLV taken at pH 7.4 in the absence (panel A), and presence (panel B) of LLP-3. Although the

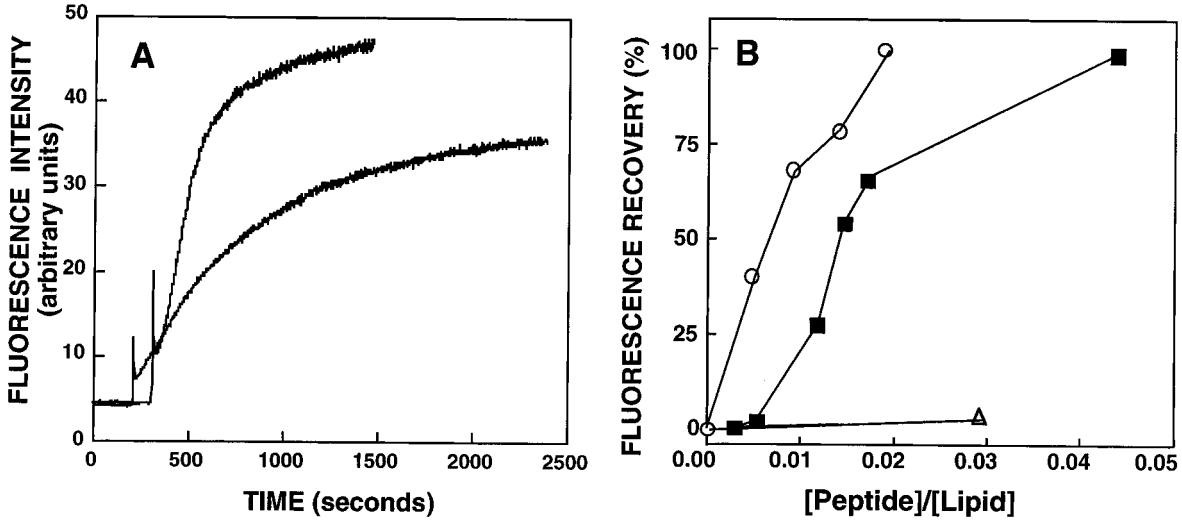

FIGURE 9: Peptide-induced dissipation of the diffusion potential in vesicles. Peptides were added to K^+ free buffer containing PC/PS/cholesterol (4:4:1 w/w) SUV (prepared in isotonic K^+ buffer), pre-equilibrated with the fluorescent dye diS-C_2-5, and valinomycin. (A) Kinetics of the fluorescence recovery upon addition of LLP-3; peptide/lipid molar ratios were 0.0146 (top) and 0.0117 (bottom). Similar results were obtained using PC/cholesterol (8:1 w/w). (B) Fluorescence recovery, measured 10 min after mixing the peptide with the vesicles, is depicted (LLP-3, filled squares). For comparison, the results obtained for the inactive V2E mutant of the fusion peptide of gp41 (open triangles) (Kliger et al., 1996) and for the neurotoxin pardaxin (open circles) (Oren & Shai, 1996) are also depicted.

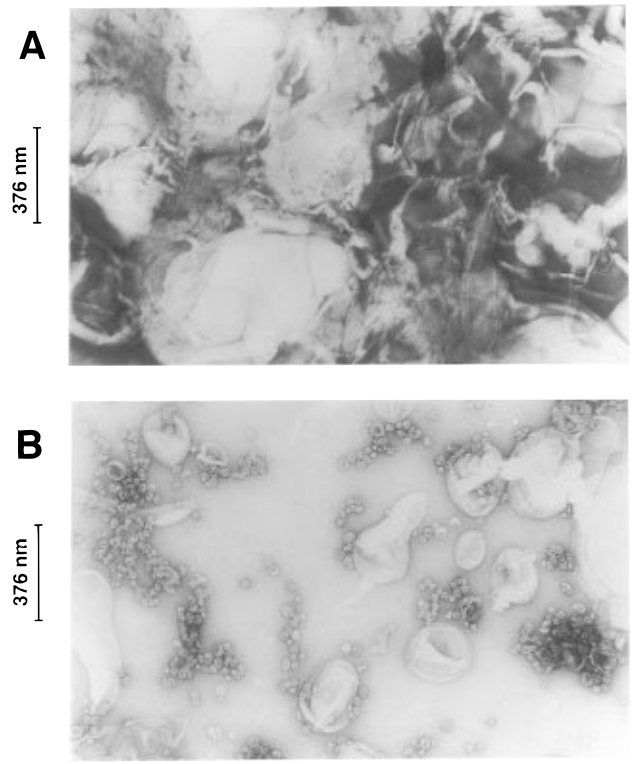

FIGURE 10: Representative micrographs of multilamellar PC/cholesterol (8:1 w/w) vesicles in the absence (A) or presence of LLP-3 peptide (B). The peptide, PC, and cholesterol were dissolved in methanol:chloroform (1:2) and then vortexed to prepare multilamellar vesicles. The procedure was done as described in Methods. Micrograph A shows multilamellar vesicles, and micrograph B shows mainly aggregates of micelles.

peptide to lipid molar ratio was very low (1:750), the micrographs show that LLP-3 interferes with the bilayer structure of MLV, inducing a non-bilayer structure consisting of aggregates of small micelles.

DISCUSSION

We have detected a leucine zipper-like sequence (leucine heptad repeat) at residues 789−815 of the cytoplasmic tail of the transmembrane envelope glycoprotein of HIV-1 (Figure 1). Heptad repeats are characterized by hydrophobic amino acids in the "a" and "d" positions of the helix. In LLP-3, all of the "a" positions are Leu and two of the "d" positions are Trp residues. Comparison of all gp41 sequences from SwissProt reveals that LLP-3 is a highly conserved sequence with respect to adjacent sequences. All the Leu residues are conserved among all the HIV-1 sequences, although there are some L to I replacements in SIV. Other heptad repeat sequences derived from viral glycoproteins identified previously have been shown to bind and interfere with the function of their parent proteins (Wild et al., 1992, 1994a, 1995; Blacklow et al., 1995; Lu et al., 1995; Rapaport et al., 1995). It has recently been shown that a heptad repeat sequence from the HIV-1 glycoprotein has a role in glycoprotein oligomerization (Bernstein et al., 1995). All of these segments are located at the ectodermal sides of their envelope glycoproteins. The sequence studied in this paper is a perfect leucine heptad repeat; unfortunately, its location in the cytoplasmic, or intra-viral, side of the membrane makes *in-vivo* investigation difficult.

In an attempt to find a role for this challenging gp41 segment in the viral life cycle, LLP-3, a 27-amino acid peptide corresponding to residues 789−815 was chemically synthesized and spectroscopically studied. Using site-specific fluorescent labeling, we found that the peptide is present in oligomeric form in aqueous solution (Figure 2). The membrane-permeating activity of fluorescently-labeled LLP-3 was tested, and results similar to that of the unlabeled peptide were obtained. A series of experiments was carried out to clarify whether LLP-3 has a role in the association of the cytoplasmic tail of gp41 with membranes.

CD and FTIR spectroscopy were used in order to determine whether LLP-3, whose primary amino acid sequence predicts α-helical secondary structure (Rost & Sander, 1993, 1994a; Rost, 1996), contains structural elements that can be modeled by the synthetic peptide. Similar results obtained with both spectroscopic methods revealed that LLP-3 adopts a 50−60% α-helical structure in its

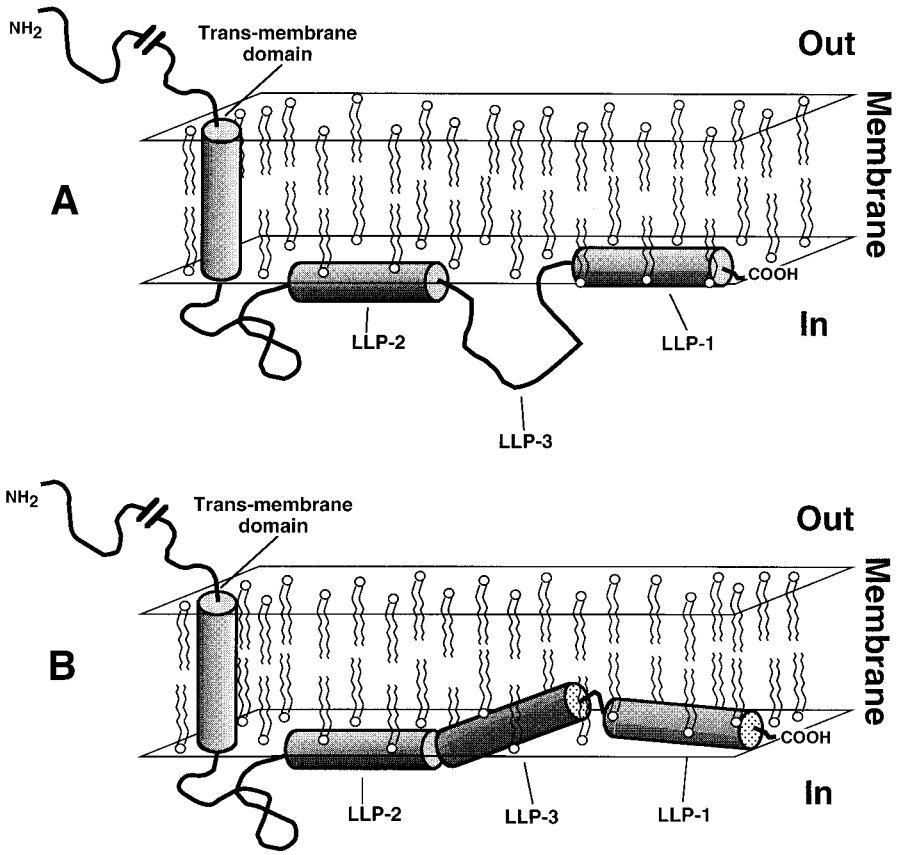

FIGURE 11: Schematic illustration suggesting a structural model for the gp41 cytoplasmic tail. In the currently accepted model (Yang et al., 1995) segments corresponding to LLP-1 and LLP-2 are in close association with the membrane bilayer (A). Our model shows a larger portion of the cytoplasmic tail in association with the cytoplasmic, intraviral side of the membrane (B).

membrane-bound state (Figure 5). In aqueous solution, there is an equilibrium between oligomeric aggregation states (Figure 2B). Within the membrane, LLP-3 oligomers dissociate into monomers. This was demonstrated by the large increase in the fluorescence of rhodamine-labeled LLP-3 following interaction with vesicles, which is equal to fluorescent levels of enzymatically-cleaved rhodamine-labeled LLP-3 (Figure 4A compared with Figure 2A), and by the lack of energy transfer between donor- and acceptor-labeled LLP-3 (Figure 4C). Further evidence comes from the finding that LLP-3 only forms monomers in SDS−PAGE (data not shown), which acts as a membrane mimetic environment (Lemmon et al., 1992; Simmerman et al., 1996). It is interesting to note that oligomeric dissociation (Figure 4A) is 3 orders of magnitude slower than LLP-3 binding to lipid vesicles (Figure 4B). All experiments performed with either zwitterionic phospholipid PC/cholesterol (8:1 w/w) vesicles or negatively-charged PS/PC/cholesterol (4:4:1 w/w) vesicles yielded similar results, indicating that the peptide−membrane interactions are mainly induced by non-electrostatic forces. This is expected because LLP-3 has no net charge at neutral pH.

This is in line of several findings which suggest that the cytoplasmic domain of gp41 is membrane-associated. (1) Two sites within the cytoplasmic domains of transmembrane HIV and SIV envelope glycoproteins are palmitoylated (Yang et al., 1995). In general, palmitoylation enhances protein association with cellular membranes. Although palmitoylation usually occurs within or close to the membrane-spanning domain (Schmidt, 1989), HIV-1 palmitoylation is approximately 59 and 132 amino acids away from the membrane-spanning domain (Yang et al., 1995). (2) There is a highly amphipathic segment, down stream and very close to the first palmitoylation site, that associates with the plasma membrane as a synthetic peptide (LLP-1, Figure 1; Fujii et al., 1992; Srinivas et al., 1992; Gawrisch et al., 1993; Miller et al., 1993a; Chernomordik et al., 1994; Tencza et al., 1995). The second palmitoylation site occurs within another highly amphipathic segment that also binds to the membrane as a synthetic peptide (LLP-2, Figure 1; Srinivas et al., 1992). The unusual large hydrophobic moments of both segments points to their association with the membrane surface (Eisenberg & Wesson, 1990). (3) A segment of the gp41 cytoplasmic domain corresponding to amino acids 839−853, which is accessible to proteinase K digestion in microsomal membranes, does not cross react with specific antibodies. The protection of this epitope from its antibody cannot be accounted for by its secondary structure or by the protein folding but only by epitope masking from lipid−bilayer interaction (Haffar et al., 1988). (4) Carbonate treatment fails to extract a polypeptide corresponding to the full-length cytoplasmic tail (residues 710−856) from the membrane fraction, suggesting that it is integrated in the lipid bilayer (Haffar et al., 1988).

Furthermore, one of the characteristic features of AIDS is a severe progressive depletion of $CD4^+$ lymphocytes, which partially explains why AIDS patients are at risk for infection by opportunistic pathogens and susceptible to specific malignant growth (Klatzmann et al., 1984; Lane et al., 1985). Several reports suggest that HIV-induced cytopathology involves the carboxyl terminus domain of gp41 (residues 707−856) which is located exclusively in the

intraviral, cytoplasmic compartment (Fisher et al., 1986; Garry, 1989; Lee et al., 1989; Haffar et al., 1991; Salzwedel et al., 1993; Miller et al., 1991, 1993a). Using ultraviolet-inactivated HIV, Garry and co-workers found that a virion component is responsible for cell killing (Rasheed et al., 1986). There are several possibilities regarding the identity of the component(s) responsible for cytopathology and cell killing, including the amino terminus fusion peptide of the transmembrane glycoprotein (Nieva et al., 1994; Kliger et al., 1996) and the two amphipathic segments from the cytoplasmic tail of the protein, corresponding to residues 768−788 and 826−854 (Fujii et al., 1992; Srinivas et al., 1992; Chernomordik et al., 1994). Our results reveal that LLP-3, a segment located between these two amphipathic segments, corresponding to amino acid residues 789−815, also has the ability to disrupt the lipid bilayer (Figures 9 and 10).

Although LLP-3's hydrophobic moment is not as striking as those of LLP-1 and LLP-2, it strongly binds membranes, is protected from enzymatic digestion in its membrane-bound state, and can perturb membranes with high potency like membrane-permeating cytolysin (Figure 9B). On the basis of the prediction of gp41 secondary structure and its accessibility to solvent (Rost & Sander, 1993, 1994a,b; Rost, 1996), it appears that a large part of the gp41 cytoplasmic domain, beginning around L-760 and ending at its carboxyl terminus, is buried in the membrane and has a high probability of α-helix formation. Two models have been proposed for the arrangement of the cytoplasmic tail of gp41: (1) the amphipathic helices, LLP-1 and LLP-2, lie on the membrane surface and do not necessarily interact with each other (Yang et al., 1995); (2) the amphipathic helices are transmembrane and are associated with each other (Venable et al., 1989). Model 1 representing HIV-1 glycoprotein as a bitopic membrane protein is the currently accepted model and is presented in Figure 11A (Berman et al., 1988; Yang et al., 1995). Our results suggest that residues 789−815 also bind to the membrane. Integration of our data with previously reported results (Haffar et al., 1988, 1991; Eisenberg & Wesson, 1990; Fujii et al., 1992; Srinivas et al., 1992; Gawrisch et al., 1993; Miller et al., 1993a; Chernomordik et al., 1994; Yang et al., 1995) suggests that a very long segment, beginning with the first palmitoylation site at Cys-764 and ending at the carboxyl terminus of the envelope glycoprotein, is membrane associated. Our findings that LLP-3 penetrates deeply into the membrane (Figures 6 and 7) and is in oblique orientation with the membrane surface (Figure 8) suggest that at least part of this segment penetrates into the hydrophobic milieu of the membrane (Figure 11B).

ACKNOWLEDGMENT

We thank Dr. Y. Marikovsky for his help in visualization of the phospholipid vesicles using electron microscopy and E. Gazit for his help with the FTIR measurements.

REFERENCES

Ben-Efraim, I., & Shai, Y. (1996) *Protein Sci. 5*, 2287−2297.
Berman, P. W., Nunes, W. M., & Haffar, O. K. (1988) *J. Virol. 62*, 3135−3142.
Bernstein, H. B., Tucker, S. P., Kar, S. R., McPherson, S. A., McPherson, D. T., Dubay, J. W., Lebowitz, J., Compans, R. W., & Hunter, E. (1995) *J. Virol. 69*, 2745−2750.
Blacklow, S. C., Lu, M., & Kim, P. S. (1995) *Biochemistry 34*, 14955−14962.
Bolen, E. J., & Holloway, P. W. (1990) *Biochemistry 29*, 9638−9643.
Bradbury, E. M., Brown, L., Downie, A. R., Elliott, A., Fraser, R. D. B., & Hanby, W. E. (1962) *J. Mol. Biol. 6*, 230−247.
Cameron, D. G., Casal, H. L., Gudgin, E. F., & Mantsch, H. H. (1980) *Biochim. Biophys. Acta 596*, 463−467.
Chernomordik, L., Chanturiya, A. N., Suss-Toby, E., Nora, E., & Zimmerberg, J. (1994) *J. Virol. 68*, 7115−7123.
De Kroon, A. I. P. M., Soekarjo, M. W., De Gier, J., & De Kruijff, B. (1990) *Biochemistry 29*, 8229−8240.
Eisenberg, D., & Wesson, M. (1990) *Biopolymers 29*, 171−177.
Fisher, A. G., Ratner, L., Mitsuya, H., Marselle, L. M., Harper, M. E., Broder, S., Gallo, R. C., & Wong-Staal, F. (1986) *Science 233*, 655−659.
Frey, S., & Tamm, L. K. (1990) *Biochem. J. 272*, 713−719.
Fringeli, U. P., & Günthard, H. H. (1981) in *Membrane Spectroscopy* (Grell, E., Ed.) pp 270−332, Springer-Verlag, Berlin.
Fujii, G., Horvath, S., Woodward, S., Eiserling, F., & Eisenberg, D. (1992) *Protein Sci. 1*, 1454−1464.
Fung, B. K., & Stryer, L. (1978) *Biochemistry 17*, 5241−5248.
Gabuzda, D. H., Lever, A., Terwilliger, E., & Sodroski, J. (1992) *J. Virol. 66*, 3306−3315.
Garry, R. F. (1989) *AIDS 3*, 683−694.
Gawrisch, K., Han, K. H., Yang, J. S., Bergelson, L. D., & Ferretti, J. A. (1993) *Biochemistry 32*, 3112−3118.
Gazit, E., & Shai, Y. (1993) *Biochemistry 32*, 12363−12371.
Gazit, E., Lee, W. J., Brey, P. T., & Shai, Y. (1994) *Biochemistry 33*, 10681−10692.
Gazit, E., Miller, I. R., Biggin, P. C., Sansom, M. S. P., & Shai, Y. (1996) *J. Mol. Biol. 258*, 860−870.
Gonzalez, M. J., Lakey, J. H., & Pattus, F. (1992) *Biochemistry 31*, 7294−7300
Haffar, O. K., Dowbenko, D. J., & Berman, P. W. (1988) *J. Cell. Biol. 107*, 1677−1687.
Haffar, O. K., Dowbenko, D. J., & Berman, P. W. (1991) *Virology 180*, 439−441.
Harrick, N. J. (1967) *Internal Reflection Spectroscopy*, Interscience Publishers, New York.
Ishiguro, R., Kimura, N., & Takahashi, S. (1993) *Biochemistry 32*, 9792−9797.
Jackson, M., & Mantsch, H. H. (1995) *Crit. Rev. Biochem. Mol. Biol. 30*, 95−120.
Kemble, G. W., Danieli, T., & White, J. M. (1994) *Cell 76*, 383−391.
Killian, J. A., Keller, R. C., Struyve, M., De Kroon, A. I. P. M., Tommassen, J., & De Kruijff, B. (1990) *Biochemistry 29*, 8131−8137.
Klatzmann, D., Barré-Sinoussi, F., Nugeyre, M. T., Danguet, C., Vilmer, E., Griscelli, C., Brun-Veziret, F., Rouzioux, C., Gluckman, J. C., Chermann, J.-C., & Montagnier, L. (1984) *Science 225*, 59−63.
Kliger, Y., Aharoni, A. Rapaport, D., Jones, P., Blumenthal, R., & Shai, Y. (1996) *Biophys. J. 70*, (2), A82.
Kowalski, M., Potz, J., Basiripour, L., Dorfman, T., Goh, W. C., Terwilliger, E., Dayton, A., Rosen, C., Haseltine, W., & Sodroski, J. (1987) *Science 237*, 1351−1355.
Lane, H. C., Depper, J. M., Greene, W. C., Whalen, G., Waldmann, T. A., & Fauci, A. S. (1985) *N. Engl. J. Med. 313*, 79−84.
Lasky, L. A., Nakamura, G., Smith, D. H., Fennie, C., Shimasaki, C., Patzer, E., Berman, P., Gregory, T., & Capon, D. J. (1987) *Cell 50*, 975−985.
Lauder, I. J., Lin, H. J., Siwak, E. B., & Hollinger, F. B. (1996) *AIDS Res. Hum. Retroviruses 12*, 91−97.
Lee, S. J., Hu, W., Fisher, A. G., Looney, D. J., Kao, V. F., Mitsuya, H., Ratner, L., & Wong-Staal, F. (1989) *AIDS Res. Hum. Retroviruses 5*, 441−449.
Lelkes, P. I., & Friedmann, P. (1984) *Biochim. Biophys. Acta 775*, 395−401.
Lemmon, M. A., Flanagan, J. M., Hunt, J. F., Adair, B. D., Bormann, B. J., Dempsey, C. E., & Engelman, D. M. (1992) *J. Biol. Chem. 267*, 7683−7689.
Levy, J. A. (1993) *Microbiol. Rev. 57*, 183−289.
Lodge, R., Göttlinger, H., Gabuzda, D., Cohen, E. A., & Lemay, G. (1994) *J. Virol. 68*, 4857−4861.

Loew, L. M., Rosenberg, I., Bridge, M., & Gitler, C. (1983) *Biochemistry 22*, 837−844.
Lu, M., Blacklow, S. C., & Kim, P. S. (1995) *Nat. Struct. Biol. 2*, 1075−1082.
Merrifield, R. B., Vizioli, L. D., & Boman, H. G. (1982) *Biochemistry 21*, 5020−5031.
Miller, M. A., Garry, R. F., Jaynes, J. M., & Montelaro, R. C. (1991) *AIDS Res. Hum. Retroviruses 7*, 511−519.
Miller, M. A., Cloyd, M. W., Liebmann, J., Rinaldo, C. R., Islam, K. R., Wang, S. Z. S., Mietzner, T. A., & Montelaro, R. C. (1993a) *Virology 196*, 89−100.
Miller, M. A., Mietzner, T. A., Cloyd, M. W., Robey, W. G., & Montelaro, R. C. (1993b) *AIDS Res. Hum. Retroviruses 9*, 1057−1066.
Miyazawa, T., & Blout, E. R. (1961) *J. Am. Chem. Soc. 83*, 712−719.
Nieva, J. L., Nir, S., Muga, A., Goñi, F. M., & Wilschut, J. (1994) *Biochemistry 33*, 3201−3209.
Oren, Z., & Shai, Y. (1996) *Eur. J. Biochem. 237*, 303−310.
Owens, R. J., & Rose, J. K. (1993) *J. Virol. 67*, 360−365.
Parente, R. A., Nir, S., & Szoka, F. C. (1990) *Biochemistry 29*, 8720−8728.
Rajarathnam, K., Hochman, J., Schindler, M., & Ferguson-Miller, S. (1989) *Biochemistry 28*, 3168−3176.
Rapaport, D., & Shai, Y. (1991) *J. Biol. Chem. 266*, 23769−23775.
Rapaport, D., & Shai, Y. (1992) *J. Biol. Chem. 267*, 6502−6509.
Rapaport, D., Ovadia, M., & Shai, Y. (1995) *EMBO J. 14*, 5524−5531.
Rapaport, D., Peled, R., Nir, S., & Shai, Y. (1996) *Biophys. J. 70*, 2502−2512.
Rasheed, S., Gottlieb, A. A., & Garry, R. F. (1986) *Virology 154*, 395−400.
Rizzo, V., Stankowski, S., & Schwarz, G. (1987) *Biochemistry 26*, 2751−2759.
Robey, W. G., Safai, B., Oroszlan, S., Arthur, L. O., Gonda, M. A., Gallo, R. C., & Fischinger, P. J. (1985) *Science 228*, 593−595.
Rost, B. (1996) *Methods Enzymol. 266*, 525−539.
Rost, B., & Sander, C. (1993) *J. Mol. Biol. 232*, 584−599.
Rost, B., & Sander, C. (1994a) *Proteins 19*, 55−72.
Rost, B., & Sander, C. (1994b) *Proteins 20*, 216−226.
Rothschild, K. J., & Clark, N. A. (1979) *Science 204*, 311−312.
Salzwedel, K., Johnston, P. B., Roberts, S. J., Dubay, J. W., & Hunter, E. (1993) *J. Virol. 67*, 5279−5288.
Schmidt, M. F. G. (1989) *Biochim. Biophys. Acta 988*, 411−426.
Schwarz, G., Stankowski, S., & Rizzo, V. (1986) *Biochim. Biophys. Acta 861*, 141−151.
Shai, Y., Bach, D., & Yanovsky, A. (1990) *J. Biol. Chem. 265*, 20202−20209.
Simmerman, H. K. B., Kobayashi, Y. M., Autry, J. M., & Jones, L. R. (1996) *J. Biol. Chem. 271*, 5941−5946.
Srinivas, S. K., Srinivas, R. V., Anantharamaiah, G. M., Segrest, J. P., & Compans, R. W. (1992) *J. Biol. Chem. 267*, 7121−7127.
Srinivas, S. K., Srinivas, R. V., Anantharamaiah, G. M., Compans, R. W., & Segrest, J. P. (1993) *J. Biol. Chem. 268*, 22895−22899.
Tencza, S. B., Miller, M. A., Islam, K., Mietzner, T. A., & Montelaro, R. C. (1995) *J. Virol. 69*, 5199−5202.
Venable, R. M., Pastor, R. W., Brooks, B. R., & Carson, F. W. (1989) *AIDS Res. Hum. Retroviruses 5*, 7−22.
Veronese, F. D., DeVico, A. L., Copeland, T. D., Oroszlan, S., Gallo, R. C., & Sarngadharan, M. G. (1985) *Science 229*, 1402−1405.
Wain-Hobson, S., Sonigo, P., Danos, O., Cole, S., & Alizon, M. (1985) *Cell 40*, 9−17.
Ward, N. E., Gravitt, K. R., & O'Brian, C. A. (1995) *Cancer Lett. 88*, 37−40.
Wild, C., Oas, T., McDanal, C., Bolognesi, D., & Matthews, T. (1992) *Proc. Natl. Acad. Sci. U.S.A. 89*, 10537−10541.
Wild, C., Dubay, J. W., Greenwell, T., Baird, T., Oas, T. G., McDanal, C., Hunter, E., & Matthews, T. (1994) *Proc. Natl. Acad. Sci. U.S.A. 91*, 12676−12680.
Wild, C., Greenwell, T., Shugars, D., Rimsky-Clarke, L., & Matthews, T. (1995) *AIDS Res. Hum. Retroviruses 11*, 323−325.
Wu, C. C. S., Ikeda, K., & Yang, J. T. (1981) *Biochemistry 20*, 566−570.
Yang, C., Spies, C. P., & Compans, R. W. (1995) *Proc. Natl. Acad. Sci. U.S.A. 92*, 9871−9875.
Yang, P. W., Stewart, L. C., & Mantsch, H. H. (1987) *Biochem. Biophys. Res. Commun. 145*, 298−302.

BI962935R